Synaptic Development of the Mouse Dorsal Lateral Geniculate Nucleus

Martha E. Bickford,[1] Arkadiusz Slusarczyk,[1] Emily K. Dilger,[2] Thomas E. Krahe,[2] Can Kucuk,[1] and William Guido[2]*

[1]Department of Anatomical Sciences & Neurobiology, University of Louisville School of Medicine, Louisville, Kentucky 40292
[2]Department of Anatomy & Neurobiology, Virginia Commonwealth University Medical Center, Richmond, Virginia 23298

ABSTRACT

The dorsal lateral geniculate nucleus (dLGN) of the mouse has emerged as a model system in the study of thalamic circuit development. However, there is still a lack of information regarding how and when various types of retinal and nonretinal synapses develop. We examined the synaptic organization of the developing mouse dLGN in the common pigmented C57/BL6 strain, by recording the synaptic responses evoked by electrical stimulation of optic tract axons, and by investigating the ultrastructure of identified synapses. At early postnatal ages (<P12), optic tract evoked responses were primarily excitatory. The full complement of inhibitory responses did not emerge until after eye opening (>P14), when optic tract stimulation routinely evoked an excitatory postsynaptic potential/inhibitory postsynaptic potential (EPSP/IPSP) sequence, with the latter having both a $GABA_A$ and $GABA_B$ component. Electrophysiological and ultrastructural observations were consistent. At P7, many synapses were present, but synaptic profiles lacked the ultrastructural features characteristic of the adult dLGN, and little γ-aminobutyric acid (GABA) could be detected by using immunocytochemical techniques. In contrast, by P14, GABA staining was robust, mature synaptic profiles of retinal and nonretinal origin were easily distinguished, and the size and proportion of synaptic contacts were similar to those of the adult. The emergence of nonretinal synapses coincides with pruning of retinogeniculate connections, and the transition of retinal activity from spontaneous to visually driven. These results indicate that the synaptic architecture of the mouse dLGN is similar to that of other higher mammals, and thus provides further support for its use as a model system for visual system development. J. Comp. Neurol. 518: 622–635, 2010.

INDEXING TERMS: thalamus; retinogeniculate; thalamocortical; corticothalamic; interneuron; triad

The dorsal lateral geniculate nucleus (dLGN) of the thalamus has served as an important model for understanding many aspects of visual system development including early pathfinding, synaptogenesis, visual map formation, and the activity-dependent refinement of synaptic connections. In recent years the mouse has become a major experimental platform for detailing key elements involved in these events. Despite the abundance of studies done in the mouse, little is known about the underlying synaptic organization of the developing dLGN.

To date, studies have focused largely on the development of retinogeniculate connections (Guido, 2008). Initially, dLGN cells are binocularly innervated and receive as many as a dozen or so separate retinal inputs. By natural eye opening (P12–P14) many of these inputs have been eliminated so that dLGN cells receive monocular innervation from just one or a few retinal ganglion cells. During this pruning phase, the remaining retinogeniculate synapses experience a several fold increase in strength (Chen and Regehr, 2000).

Little is known regarding the ultrastructural changes underlying these events. In adult tissue, retinal terminals in the dLGN have been well studied and are quite distinct (Szentagothai et al., 1966; Guillery, 1969; Guillery, 1971; Robson and Mason, 1979; Hamos et al., 1987). They are known as RLP profiles because of their *round* shaped vesicles, *large* size, and *pale* mitochondria. Indeed, retinal ter-

Grant sponsor: National Institute of Neurological Disorders and Stroke; Grant numbers: NS35377; Grant sponsor: National Eye Institute: Grant numbers: EY016155 (to M.E.B.) and EY12716 (to W.G.); Grant sponsor: the Society for Neuroscience; Grant: grant to aid investigators affected by Hurricane Katrina.

*CORRESPONDENCE TO: William Guido, Department of Anatomy and Neurobiology, Virginia Commonwealth University Medical Center, Richmond, VA 23298. E-mail: wguido@vcu.edu

Received 23 May 2009; Revised 5 August 2009; Accepted 5 September 2009
DOI 10.1002/cne.22223
Published online September 16, 2009 in Wiley InterScience (www.interscience.wiley.com).

minals are the largest terminals in the dLGN, and each bouton forms multiple synaptic contacts (Rafols and Valverde, 1973; Rapisardi and Miles, 1984; Wilson et al., 1984). Whether these features are apparent at early ages, and how the remodeling process takes shape at the ultrastructural level, remain unexplored.

Adult retinogeniculate terminals also contact dendritic terminals (F2 profiles), which have been identified as originating from interneurons (Famiglietti, 1970; Famiglietti and Peters, 1972; Rafols and Valverde, 1973; Lieberman and Webster, 1974; Hamos et al., 1985) that utilize γ-aminobutyric acid (GABA) as a neurotransmitter (Montero and Singer, 1985; Montero, 1991; Fitzpatrick et al., 1984). Unique "triadic" arrangements are formed when a single retinal terminal is presynaptic to both a relay cell dendrite and an F2 profile, which are themselves connected by a synapse. These arrangements often occur within a glomerulus, a complex zone of multiple synapses encased by a glial sheath (Sherman, 2004).

In other species, approximately 20% of the retinogeniculate synapses are formed with F2 profiles and the remainder with relay cell dendrites (Wilson and Hendrickson, 1981; Erisir et al., 1998; Van Horn et al., 2000; Datskovskaia et al., 2001; Li et al., 2003). However, although triadic arrangements have been identified in the adult mouse dLGN (Rafols and Valverde, 1973), it is not clear how prevalent these synapses are, because mice have far fewer intrinsic interneurons than higher mammals (Arcelli et al., 1997). It is also not clear when they first appear during development because the maturation of some inhibitory synapses in the rodent thalamus is delayed until postnatal ages (DeBiasi et al., 1997; Ziburkus et al., 2003).

Finally, although retinal inputs provide the primary excitatory drive for dLGN cells, most of the synaptic connections in the dLGN arise from nonretinal sources (Sherman and Guillery, 2002). In the adult dLGN, the cortex and brainstem provide glutamatergic and cholinergic inputs, respectively (Erisir et al., 1997a,b), in the form of *small* profiles with densely packed *round* vesicles and *dark* mitochondria (RSD profiles). Additional GABAergic inputs arise from the thalamic reticular nucleus (TRN), pretectum, and interneuron axons in the form of medium-sized terminals that contain densely packed vesicles (F1 profiles), distinguishing them from the more loosely packed vesicles contained within F2 profiles (Ohara et al., 1980; Montero and Scott, 1981; Fitzpatrick et al., 1984; Wilson et al., 1984; Hamos et al., 1985; Montero and Singer, 1985; Cucchiaro et al., 1991a,b; Arcelli et al., 1997; Wang et al., 2001; Wang et al., 2002; Li et al., 2003). However, little if anything is known about how, where, and when these connections emerge or coordinate with the refinement of retinogeniculate connections.

To address these questions, we explored the synaptic organization of the developing mouse dLGN in the common pigmented C57/BL6 strain, first by recording the synaptic responses evoked by electrical stimulation of optic tract axons, and second by examining the ultrastructure of identified synapses. To aid in the characterization of inhibitory elements, we also made use of postembedding immunocytochemical staining for GABA.

MATERIALS AND METHODS

Electrophysiology

To examine the synaptic responses evoked by optic tract stimulation, an acute thalamic slice preparation was adopted in which the retinal connections to the dLGN as well as inhibitory intrinsic connections within the LGN remain intact (Chen and Regehr, 2000). C57/BL6 mice, ranging in age from postnatal day (P) 7 to 34 were anesthetized with isoflurane and decapitated. The brain was removed from the skull, and the two hemispheres were separated by cutting along the midline at an angle of 10–20°. The medial aspect of the brain was then glued onto an angled wedge (15–25°) of a Vibratome cutting stage and submerged in a 4°C oxygenated (95% O_2/5% CO_2) sucrose solution (in mM: 26 $NaHCO_3$, 23.4 sucrose, 10 $MgSO_4$, 0.11 glucose, 2.75 KCl, 1.75 Na $H2PO_4$, 0.5 $CaCl_2$, saturated with 95% O_2/5% CO_2). Using a Vibratome (Leica 2000), 250–300-μm-thick sections were cut in the parasagittal plane.

Slices containing the dLGN were placed in a holding chamber and incubated with artificial cerebral spinal fluid (ACSF; in mM: 124 NaCl, 2.5 KCl, 1.25 NaH_2PO_4, 2.0 $MgSO_4$, 26 $NaHCO_3$, 10 glucose, 2 $CaCl_2$, saturated with 95% O_2/5% CO_2, pH 7.4) at 30–35°C for 1 hour. Individual slices were then transferred to a recording chamber maintained at 32°C and perfused continuously at a rate of 2.0 ml/min with oxygenated ACSF. In vitro recordings were done in a whole cell configuration with the aid of a fixed-stage microscope (Olympus EX51WI or Nikon E600FN) equipped with differential interference contrast optics and a water-immersion objectives to view individual neurons within the slice. Patch electrodes were pulled vertically in two stages from borosilicate glass and filled with a solution containing (in mM) 140 K gluconate, 10 HEPES, 0.3 NaCl, 2 ATP-Mg, 0.1 GTP-Na (pH 7.25, 260 OSM). The final tip resistance of filled electrodes was 3–5 MΩ. Whole cell recordings were done in current clamp mode by using an Axoclamp 2B amplifier (MDS, Mississauga, ON, Canada). Pipette capacitance, series resistance, and whole cell capacitance were carefully monitored and compensated electronically during the recording. To evoke synaptic activity in dLGN, square-wave pulses (0.1–0.3 ms, 0.1–1 mA) were delivered at a rate of 0.2–1.0 Hz through a pair of thin-gauge tungsten wires (0.5 MΩ) positioned in the optic tract.

To ensure that we evoked all direct monosynaptic excitatory connections as well as di-synaptic feedforward inhibitory ones, we used a range of stimulus intensities that evoked threshold, suprathreshold, and maximal responses. GABA antagonists bicuculline (25 μM; Tocris, Ellisville, MO) and CGP (10 μM, Tocris) were bath-applied to isolate $GABA_A$- and $GABA_B$-mediated activity, respectively. Neuronal activity was digitized (10–20 KHz) through an interface unit (National Instruments, Baltimore, MD), acquired and stored directly on the computer, and analyzed by using commercial software (Strathclyde, Glasgow, Scotland; Electrophysiology Software, Whole Cell Analysis Program V3.8.2.)

Electron microscopy

To examine the ultrastucture of the developing dLGN, a total of eight C57/BL6 mice, at ages P7 (n = 2), P14 (n = 2), P21 (n = 2), and adult (9 months, n = 2) were used. Mice were first deeply anesthetized with isoflurane, then given an intraperitoneal injection of avertin (2.5%, 0.5–1 ml), and perfused through the heart with 2% paraformaldehyde and 2% glutaraldehyde in 0.1 M phosphate buffer. The brains were cut into 50–100-μm-thick coronal sections by using a Vibratome (Leica VT100E). Selected sections were postfixed in 2% osmium tetroxide and then dehydrated in an ethyl alcohol series and embedded in Durcupan resin. Because the mouse dLGN is less than 1 mm^2 in coronal sections, we mounted the entire dLGN (at its largest extent, approximately 2.3 mm posterior to Bregma in the adult) on resin blocks for ultrastructural analysis. Ultrathin sections (on average 70 nm in thickness) were cut and every fifth section was collected on Formvar-coated nickel slot grids. Every fourth section in the series was stained to reveal the presence of GABA, by using previously published postembedding immunocytochemical techniques (Li et al., 2003; Bickford et al., 2008) and a polyclonal, affinity-purified rabbit anti-GABA primary antibody (cat. no. A2052, Sigma, St. Louis, MO) diluted 1:2,000, and a goat anti-rabbit IgG antibody conjugated to 15-nm colloidal gold particles diluted 1:25 (British BioCell International, Cardiff, UK).

The immunogen used to produce the GABA antibody was GABA-bound to bovine serum albumin (BSA). The GABA antibody shows positive binding with GABA and GABA-keyhole limpet hemocyanin, but not BSA, in dot blot assays (Sigma product information). In mouse tissue, the GABA antibody stains neurons in the thalamic reticular nucleus and a subset of neurons in the dorsal thalamus. This labeling pattern is consistent with other GABAergic markers used in a variety of species to visualize interneurons. (Houser et al., 1980; Hendrickson et al., 1983; Oertel et al., 1983; Fitzpatrick et al., 1984; Montero and Singer, 1985; Montero and Zempel, 1986; Rinvik et al., 1987; De Biasi et al., 1997; Arcelli et al., 1997; Wang et al., 2001).

The sections were subsequently stained with uranyl acetate and examined by using a Philips CM10 electron microscope. Images of each synaptic contact (identified by an accumulation of vesicles adjacent to a synaptic cleft) encountered within the examined sections were collected by using a digitizing camera (SIA-7C; SIA, Duluth, GA), or photographic plates that were subsequently scanned and digitized (SprintScan 45i; Polaroid, Waltham, MA). As described in detail in the Results section, each presynaptic and postsynaptic profile was categorized based on a variety of ultrastructural features, as well as the density of gold particles overlying them. Profile areas were measured from digital images of single sections by using Sigma Scan Software (SPSS, Chicago, IL). Images were imported into Adobe Photoshop software (San Jose, CA), where the brightness and contrast could be adjusted.

RESULTS

Development of retinogeniculate postsynaptic potentials

We studied the synaptic responses evoked by optic tract stimulation from a total of 91 relay cells at ages ranging from P7 to 34. Representative examples from different postnatal ages are shown in Figure 1. At early postnatal ages, synaptic responses were primarily excitatory postsynaptic potentials (EPSP), comprised of large, long-lasting depolarizations (Fig. 1A). Although weak inhibitory postsynaptic potentials (IPSP) were apparent in some cells as early as P9 (Fig. 1A), the full complement of IPSP activity did not emerge until after eye opening (>P14). As is the case for mature rodent dLGN cells (Crunelli et al., 1988; Ziburkus and Guido, 2003; Blitz and Regehr, 2005), the synaptic responses were comprised of an EPSP followed by IPSP activity. As shown in Figure 1B and C, inhibitory responses often contained two distinct hyperpolarizing components, an early, short-duration IPSP that was blocked by the $GABA_A$ antagonist bicuculline, and a slower, long-duration IPSP that was blocked by the $GABA_B$ antagonist CGP.

With increasing age, the GABA-mediated responses greatly attenuated the amplitude and duration of the preceding EPSP (Fig. 1C,D). Figure 1D plots the incidence of inhibition as a function of age for 91 cells. Between P7 and 11, inhibition was rare (20%) but increased steadily with age so that by P16–20 close to 83% of all cells showed some form of inhibition evoked by optic tract stimulation. During the third and fourth postnatal week (P21–34) virtually all cells (93%) exhibited inhibitory responses. Pairwise comparisons reveal a significant increase in the incidence of inhibition with age (Fisher's exact test; P7–11 vs

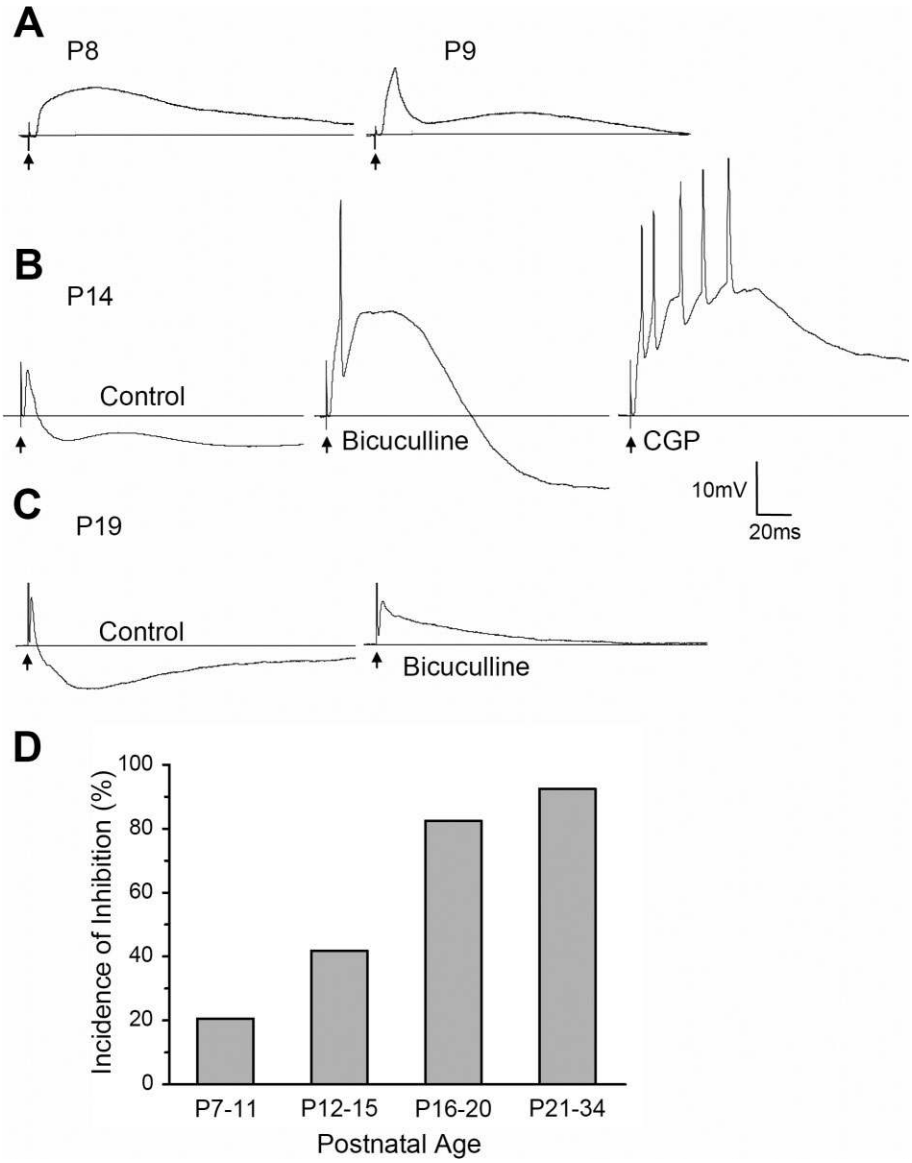

Figure 1. Postsynaptic responses evoked by optic tract stimulation in the developing mouse dLGN. A–C: Examples of synaptic responses recorded at different postnatal ages (P). **A:** Between P7 and 11, synaptic responses are largely excitatory. *Left:* Example of a pure EPSP recorded at P8. *Right:* Example of an EPSP followed by a small IPSP at P9. **B:** At older ages (>P12) inhibition was more pronounced and contained a $GABA_A$ and $GABA_B$ component. Example of synaptic responses recorded at P14 before (control ACSF, *left*) and after bath application of the $GABA_A$ antagonist bicuculline (25 μM, *middle*) and $GABA_B$ antagonist CGP (10 μM, *right*). Initially, the response contained an EPSP followed by IPSP activity that had two hyperpolarizing components: an early fast one ($GABA_A$) followed by a somewhat slower long-duration one ($GABA_B$). Bicuculline blocked the early hyperpolarizing response and unmasked a high-amplitude, long-duration EPSP. CGP blocked the additional slower, long-lasting hyperpolarization, leading to a further increase in the duration of the preceding EPSP. **C:** Example of a response at P19 before (*left*) and after (*right*) bath-applied bicuculline. The IPSP activity greatly curtailed the duration of the initial EPSP **D:** Summary plot showing the incidence of synaptic responses containing inhibition at different postnatal ages. There was an age-related increase in the incidence of inhibition. The number of cells recorded at each age group were: P7–11, n = 24; P12–15, n = 31; P16–20, n = 23; P21–34, n = 13. In A–C, responses were recorded at −60–mV, and arrows indicate stimulus artifacts.

P12–15 $P < 0.003$; P12–15 vs P16–20 $P < 0.001$; P16–20 vs P21–34 $P < 0.03$).

Development of dLGN synapse ultrastructure

For ultrastructural analysis we examined a total of 2,128 synapses in the dLGN at P7 (n = 146), P14 (n = 872), P21 (n = 217), and adult (n = 893). Representative examples of the synaptic profiles found in the dLGN are shown in Figures 2, 4, 5, and 8.

At P7, synapses were easily identified, although the ultrastructure of the dLGN was quite immature; synaptic profiles that are readily identified in adult tissue were not

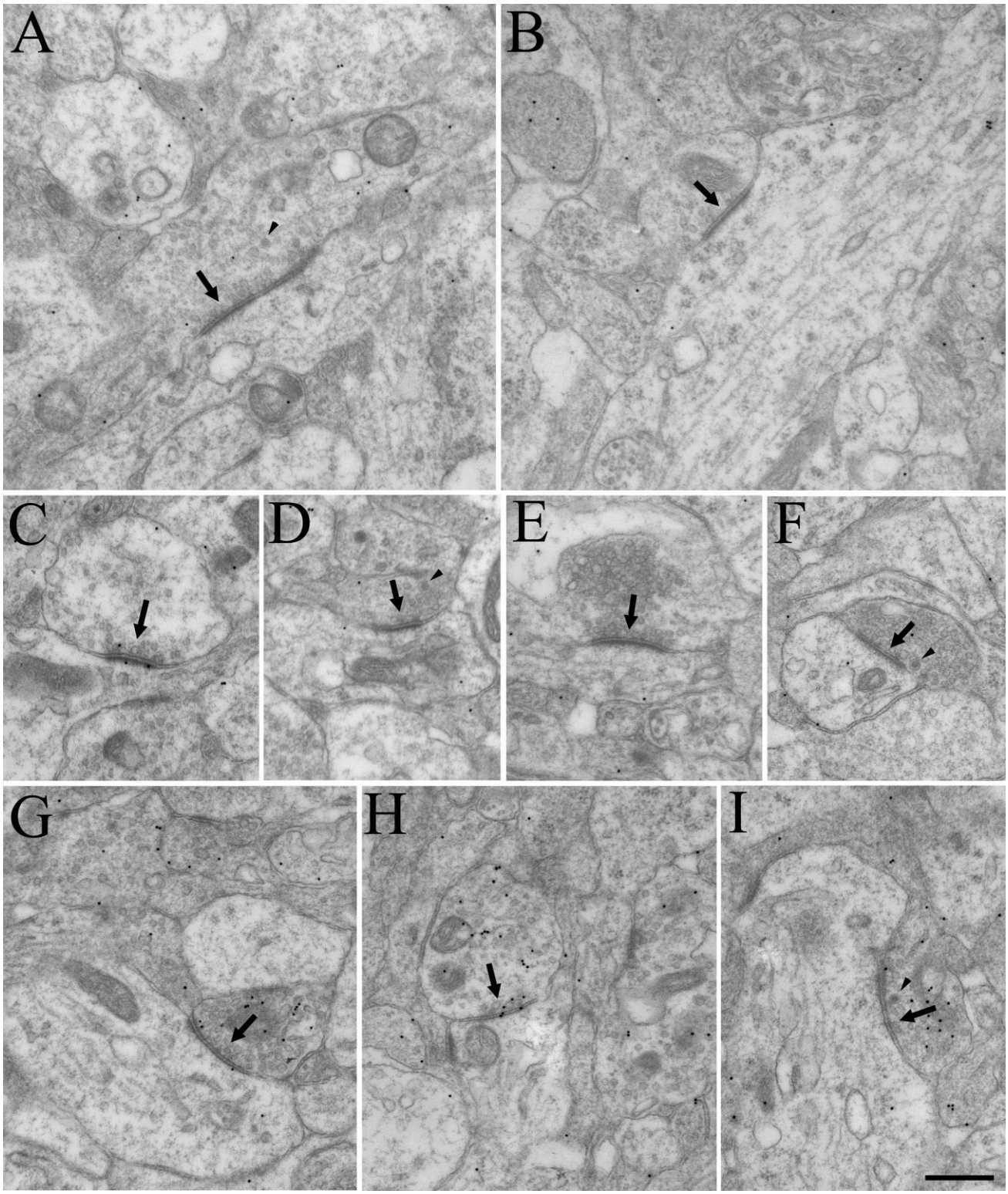

Figure 2. Electron micrographs depict the synaptic architecture of dLGN at P7. Although synapses could be easily identified (arrows, A–I), specific types of terminals could not be categorized based on ultrastructure. Pale mitochondria could not be definitively identified, and vesicles were in general, sparsely distributed (**A–F**). Dense-core vesicles (arrowheads) were frequently observed, but did not appear to correlate with other ultrastructural features. Although there was some specificity in the distribution of gold particles overlying presynaptic profiles (**G–I**), the staining for GABA was sparse and indistinct. Scale bar = 0.5 μm in I (applies to A–I).

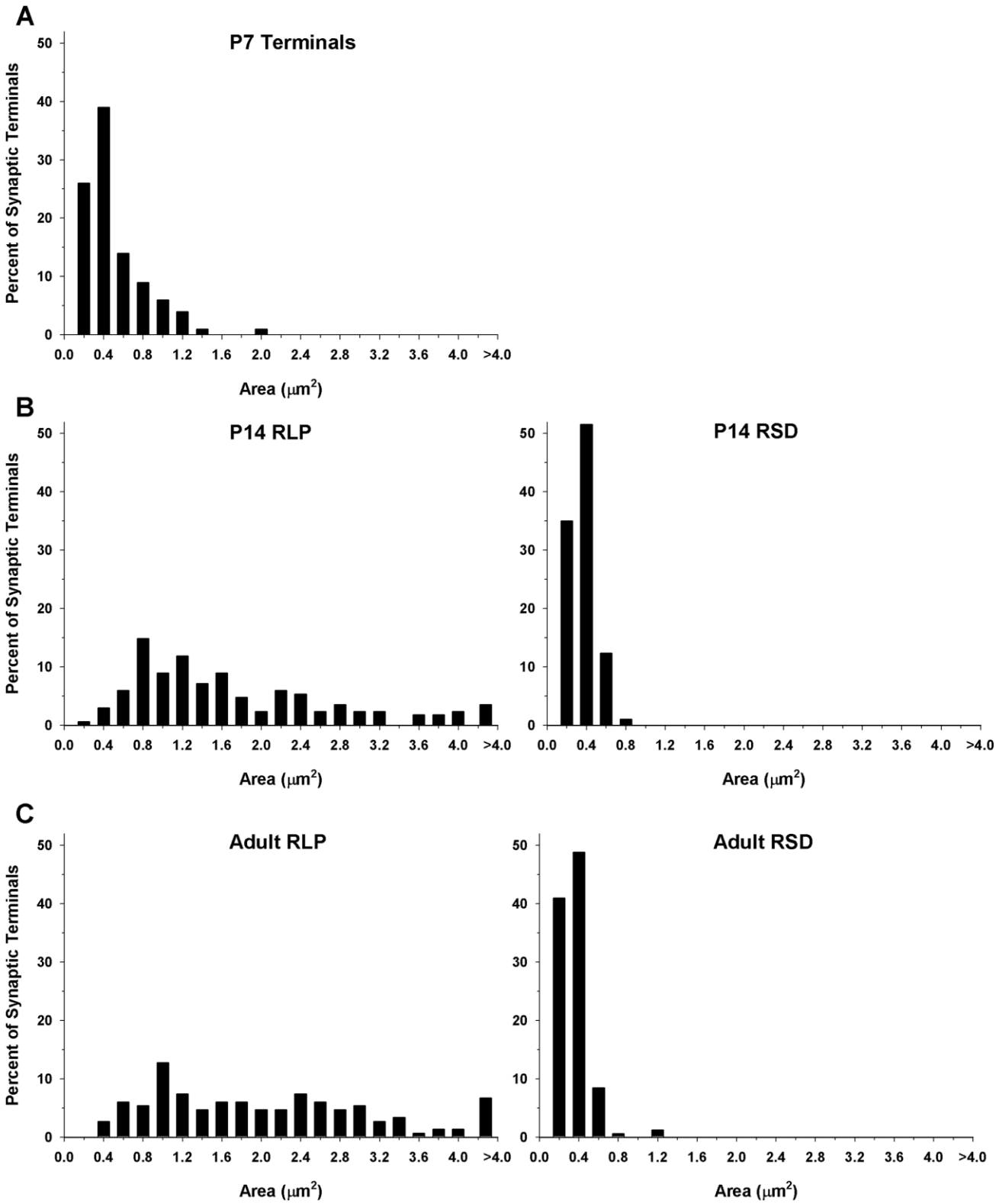

Figure 3. Frequency histogram illustrates the distribution of terminal sizes in dLGN at P7 (**A**), P14 (**B**), and adult (**C**). The sizes of RLP (large profiles that contain round vesicles and pale mitochondria) and RSD profiles (small profiles that contain round vesicles and dark mitochondria) were similar in the P14 and adult dLGN. Synaptic terminals types cannot be distinguished at P7, and were smaller than RLP profiles identified at later ages. At P7, n = 100 terminals; P14, n = 97 RSD and n = 168 RLP; adult, n = 166 RSD and n = 149 RLP profiles.

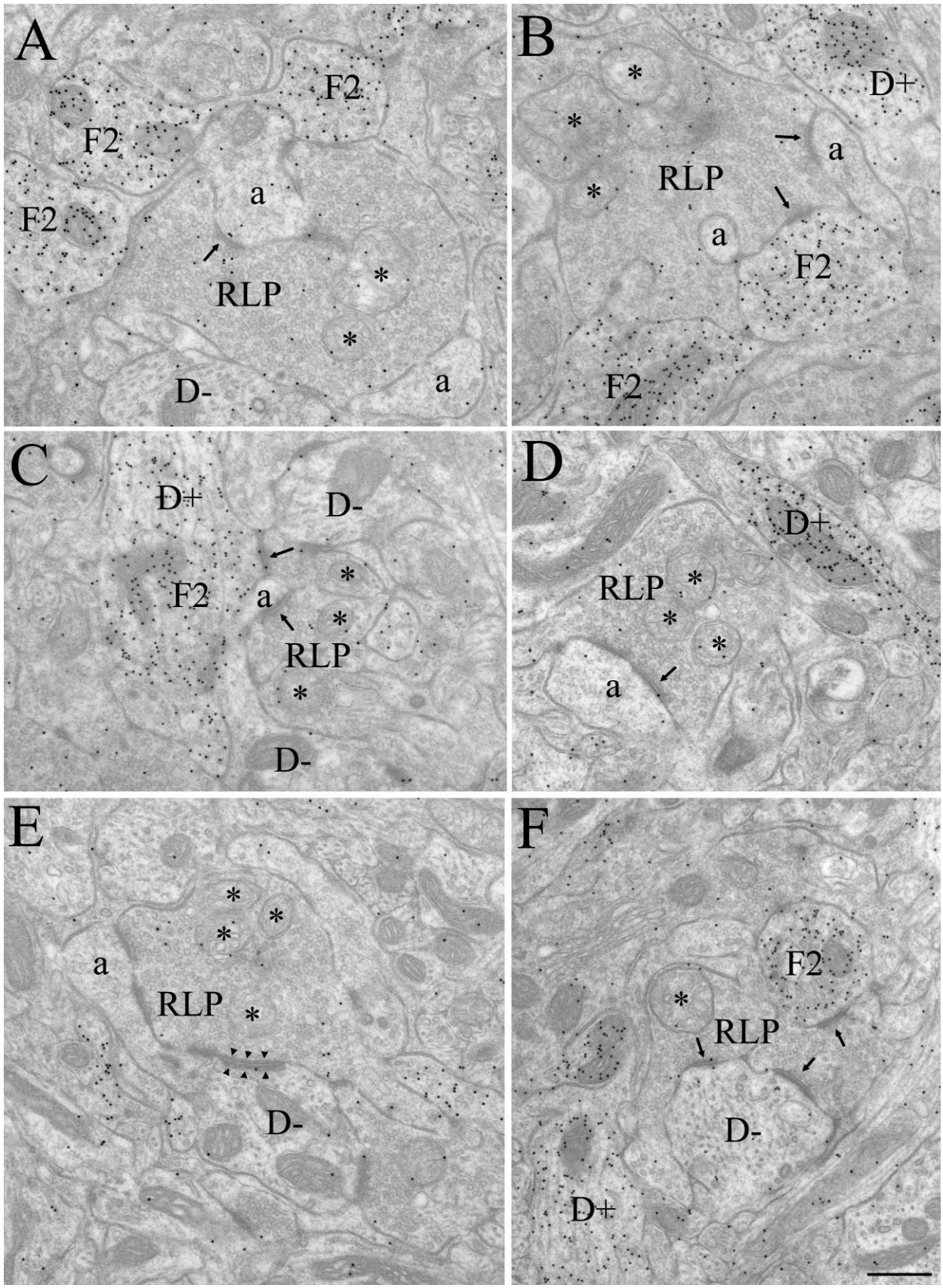
A
F2
F2
F2
a
RLP
D-
a
B
D+
a
RLP
a
F2
F2
C
D+
D-
F2
a
RLP
D-
D
D+
RLP
a
E
a
RLP
D-
F
F2
RLP
D-
D+

Figure 4

apparent (Fig. 2). In particular, RLP profiles could not be distinguished. As shown in Figure 3, which plots the distribution of terminal sizes at different ages, the synaptic profiles at P7 were significantly smaller (Mann-Whitney U = 23.5, $P < 0.04$; P7 median = 0.34 μm^2) than RLP profiles identified at older ages (P14 median 1.33 μm^2, adult median 1.74 μm^2). The ultrastructure of mitochondria within synaptic profiles was relatively homogeneous. Dense-core vesicles were often observed within synaptic terminals but could not be used to distinguish terminal types (arrowheads, Fig. 2A,D,I). Likewise, RSD profiles could not be identified with any confidence at P7. Although a few synaptic profiles in the P7 dLGN contained numerous vesicles (Fig. 2E,F), in most synaptic terminals the vesicles were quite sparse (Fig. 2C). Finally, although a few synaptic profiles were found to contain a higher density of gold particles than those of surrounding profiles (Fig, 2G–I), there was insufficient accumulation of GABA in P7 synaptic profiles to confidently classify them as GABAergic and non-GABAergic by using our immunocytochemical techniques (Li et al., 2003).

In contrast, by P14 profiles were easily recognized in the dLGN, and GABA staining was robust (Figs. 4, 5). RLP profiles could be identified by their distinctive pale mitochondria (Fig. 4, asterisks), and relatively large size (median 1.33 μm^2). RSD profiles also were evident based on their densely packed vesicles, prominent postsynaptic densities (Fig. 5B–D), and relatively small size (median 0.22 μm^2). Indeed, at P14, both RLPs and RSD profiles were adult-like in composition and overall size. As shown in Figure 3, the overall distributions of terminal size for RLP and RSD profiles measured in P14 and adult tissue were not significantly different from each other (Mann-Whitney U = 47, $P < 0.820$; U = 46, $P < 0.691$). Finally, GABAergic profiles were readily distinguished by the high density of gold particles contained within them compared with surrounding structures. Both F1 (Fig. 5E–G) and F2 profiles (Fig. 4A–C,F), as well as GABAergic somata (S+; Fig. 5A) and dendritic shafts (D+; Figs. 4B–D,F, 5B) were well delineated.

We compared the distribution of synaptic terminals that could be characterized at P14 with those found in the adult. For these comparisons, digital image montages of single sections were collected, and then for all identifiable synaptic contacts the presynaptic profiles were categorized based on GABA staining and morphology. Although F1 and F2 profiles could be identified in both P14 and adult tissue, the density of vesicles within each category can vary, and not all F2 profiles are postsynaptic in any given section. Therefore, we simply placed presynaptic profiles into one of four categories: RLP, RSD, GABAergic, or those that could not be classified (Un). Unclassified synapses included those in which either the section did not contain enough of the presynaptic profile to provide adequate morphological criteria for categorization, or the morphology did not fit one of the categories described above. For example, a few non-GABAergic profiles were large but did not contain pale mitochondria, or the vesicle density was lower than that typically observed in RSD or RLP profiles.

As illustrated in Figure 6, in the P14 (n = 585) and adult dLGN (n = 558), RSD synapses make up the vast majority of the total synaptic contacts (61.88–65.95%). RLP synapses comprise only 11.65–13.85%, and GABAergic synapses comprise 16.49–18.63% of the total synaptic contacts. The percentage of unclassified presynaptic profiles was small and similar for both P14 and adult tissue (5.64% for P14 and 5.91% in the adult).

Finally, we classified the postsynaptic targets of RLP profiles in tissue from P14, P21, and adult mice. As shown in Figure 7, the proportion of GABAergic and non-GABAergic profiles targeted by retinogeniculate terminals was similar. At each age, approximately 10% of the profiles postsynaptic to retinogeniculate terminals were classified as GABAergic F2 profiles, and the rest were non-GABAergic dendrites. RLP profiles rarely contacted somata. In fact, at all ages, the vast majority of identified synaptic contacts were made onto dendrites; extremely few somatic contacts were observed.

Development of dLGN glomeruli

Although there were no quantitative changes in the size and distribution of identified terminal types in the dLGN at P14, P21, and adult, a few qualitative observations deserve mention. First, in adult tissue, the synaptic arrangements of retinal terminals appeared to be more isolated from the adjacent neuropil than those in developing tissue (Fig. 8). Although not readily quantified, this isolation was due to an apparent increase in glial lamellae that surround

Figure 4. Electron micrographs illustrate the synaptic architecture of the P14 dLGN. At this age, retinal terminals were readily identified as RLP profiles (**A–F**), i.e., large profiles that contain round vesicles and pale mitochondria (*). RLP profiles contacted (arrows) non-GABAergic dendrites (D-), identified by a low density of gold particles, the presence of microtubules and occasional mitochondria, and the absence of synaptic vesicles (A,C,E,F). RLP profiles also contacted non-GABAergic dendritic appendages (a), identified as small profiles that contained diffusely organized neurofilaments, no microtubules, few mitochondria, a low density of gold particles, and no synaptic vesicles (A–E). Appendages were often observed to invaginate RLP profiles (B). RLP profiles also contacted F2 profiles (identified as profiles that contain loosely packed synaptic vesicles and a high density of gold particles (A–C,F). In C, an F2 profile originated from a GABAergic dendrite (D+), identified by the presence of microtubules and occasional mitochondria, a high density of gold particles, and few or no synaptic vesicles (C,D,F). RLP profiles also formed occasional adherent contacts with adjacent profiles (arrowheads, illustrated in E). Scale bar = 0.5 μm in F (applies to A–F).

glomeruli (white arrows, Fig. 8), a feature that is consistent with Guillery's (1969) original definition of glomeruli.

Puncta adherentia, the desmosome-like contacts between dLGN profiles, are also particularly prominent within adult glomerular structures (Patel and Bickford, 1997). These contacts are identified by prominent densities on each side of adjacent profiles, and a widened space between the adjacent membranes (similar to a synaptic cleft). However, although the overall appearance of puncta adherentia is similar to a synapse, vesicles are absent from the vicinity of the junction. In P14 tissue, adherent junctions were occasionally identified, but formed single, longer contacts (Fig. 4E, arrowheads) rather than the multiple punctate junctions seen in adult tissue (Fig. 8, arrowheads). In an attempt to quantify this developmental change, we counted the number of adherent junctions in the montages used to quantify synapses. For this analysis, multiple adjacent puncta adherentia connecting two profiles were counted as one junction. Because virtually all adherent contacts are formed between RLP profiles and their postsynaptic partners, we compared the number of RLP adherent junctions with the number of RLP synaptic contacts identified at each age. This analysis revealed a developmental increase in the ratio of adherent junctions to synaptic contacts associated with retinal terminals (P14 RLP adherent junctions/synaptic contacts = 0.33, adult = 1.02).

DISCUSSION

Our results indicate that most of the ultrastructural features characteristic of the adult dLGN cannot be recognized at P7. Although many synapses are present, they could not be readily classified. Overall profiles appeared immature. They were relatively small and uniformly shaped and contained homogenous mitochrondria, sparse synaptic vesicles, and little detectible GABA. Because these are the primary features used to distinguish synaptic profiles in the adult, it is difficult to discern the source of synaptic input in neonatal dLGN based on morphology per se. However, it seems likely that the synaptic terminals present at P7 are primarily of retinal origin, and most synapses are formed between retinogeniculate terminals and the dendrites of relay cells. This conclusion is based on three observations.

First, in P7 dLGN tissue the GABA concentrations were too low to confidently distinguish profile types, suggesting a paucity of well-defined inhibitory elements (DeBiasi et al., 1997). Second, our in vitro recordings revealed that until P12 optic tract stimulation evokes mainly excitatory postsynaptic responses in the dLGN. The failure to detect inhibitory responses at earlier postnatal ages suggests that synapses between interneurons and relay cells have not yet developed (Ziburkus and Guido, 2003).

Finally, although we did not explore whether electrical activation of corticothalamic (CT) axons could evoke postsynaptic activity in neonatal dLGN, it is unlikely that such synapses are present, because CT axons do not fully innervate the mouse dLGN until about 2 postnatal weeks (Jacobs et al., 2007). In contrast, mouse retinal ganglion cell axons innervate dLGN at embryonic ages (Godement et al., 1984), and at early postnatal ages, they provide the primary excitatory drive to relay cells (Mooney et al., 1996).

By P14 the synaptic organization of the dLGN has fully matured, and the ultrastructure of synaptic profiles could be readily classified. Importantly, we were able classify the same percentage of profiles in P14 and adult tissue, suggesting that by P14 most profiles have acquired their adult-like characteristics, and few if any immature profiles remain. Of course, tract tracing coupled with immunocytochemistry may be necessary for unequivocal terminal identification and for a thorough characterization of the morphological transformations that distinguish developing retinal, cortical, and brainstem terminals in the dLGN .

As in the adult dLGN (Rafols and Valverde, 1973), P14 RLP profiles contacted both non-GABAergic relay cells dendrites and the dendritic terminals of GABAergic interneurons (F2 profiles). Thus all the elements of adult triadic arrangements (in which a single retinal terminal is presynaptic to both a relay cell dendrite and an F2 profile, which are themselves connected by a synapse), are present at 2 weeks of age. The appearance of these synaptic contacts is consistent with our electrophysiological observations. Weak inhibitory responses begin to appear just after the first postnatal week, and then increase steadily with age so that by P14–16 large IPSPs mediated by both $GABA_A$ and $GABA_B$ receptors are almost always evoked by optic tract simulation. Optic tract-evoked IPSP activity was also tightly coupled to a preceding EPSP (Ziburkus and Guido, 2003; Jaubert-Miazza et al., 2005). This EPSP/IPSP sequence reflects the concerted activation of synapses that comprise a triad, and has been referred to as feedforward "locked" inhibition, which increases the temporal precision of retinogeniculate signal transmission (Blitz and Regehr, 2005).

At P14 other inhibitory elements are also present and appear to form mature synaptic relationships. In particular F1 profiles, which in other species have been shown to arise from the TRN, pretectum, or intrinisic interneurons axons (Ohara et al., 1980; Montero and Scott, 1981; Fitzpatrick et al., 1984; Wilson et al., 1984; Hamos et al., 1985; Montero and Singer, 1985; Cucchiaro et al., 1991a,b; Arcelli et al., 1997; Wang et al., 2001; Wang et al., 2002; Li et al., 2003), are readily identified by their densely packed synaptic vesicles and intense immunocytochemical staining for GABA. These elements provide a

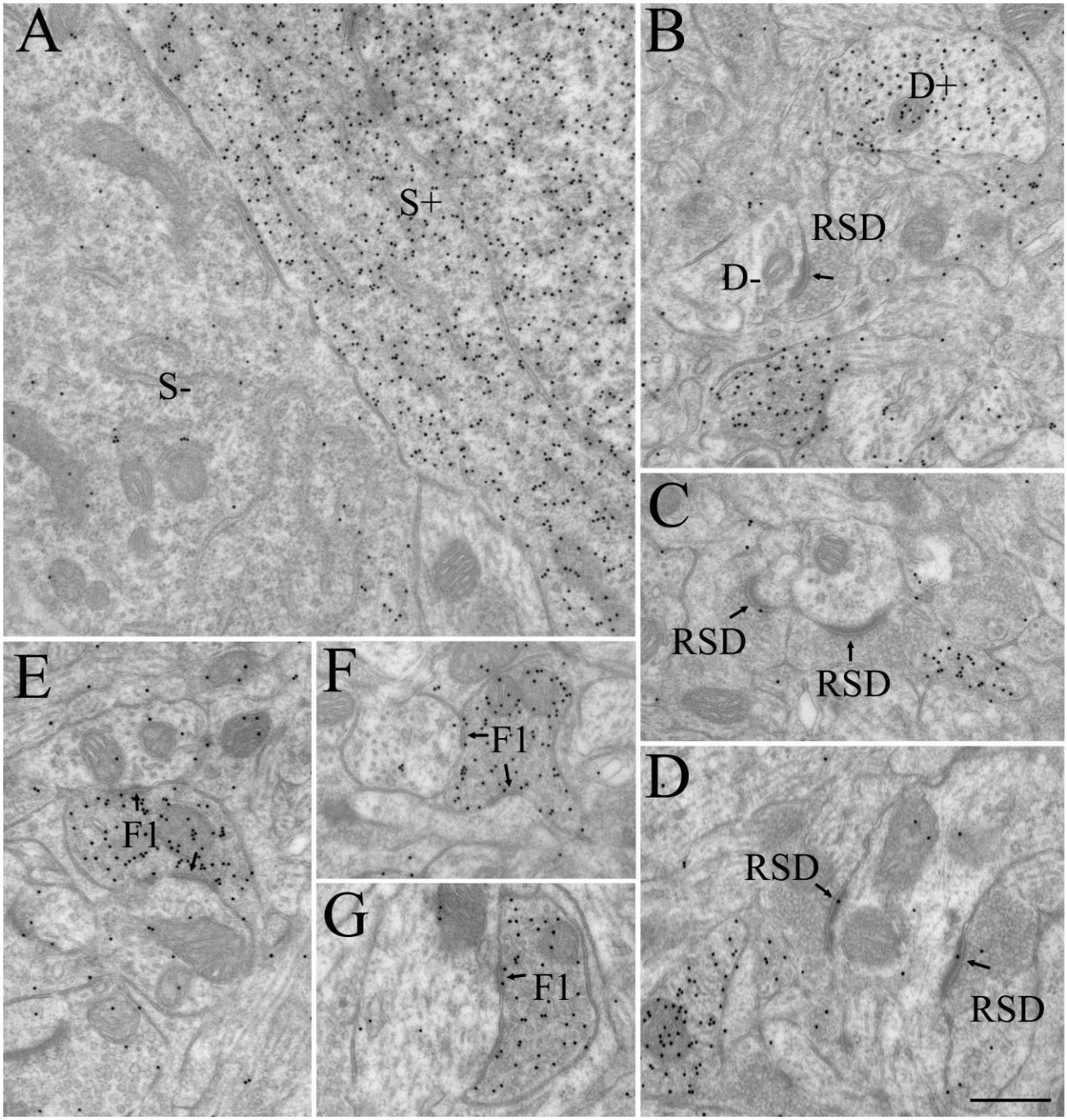

Figure 5. Electron micrographs illustrate GABAergic and non-GABAergic profiles at P14. These were distinguished based on differences in the density of overlying gold particles. **A:** Adjacent GABAergic (S+) and non-GABAergic (S-) somata. **B:** GABAergic (D+) and non-GABAergic (D-) dendrites. RSD profiles were identified as small non-GABAergic terminals that contained densely packed vesicles and formed asymmetric synapses (arrows; **B–D**). F1 profiles were identified as GABAergic terminals that contained densely packed vesicles and formed symmetric synapses (arrows; **E–G**) Scale bar = 0.5 μm in D (applies to A–G).

variety of forms of feedforward and feedback inhibition onto relay cells, serving to shape receptive field structure or gate signal transmission (Sherman and Guillery 2002; Sherman, 2005).

The relatively late appearance of F1 profiles in the mouse dLGN is consistent with the emergence of inhibitory elements in other thalamic structures. For example, in rodents, GABA profiles in ventrobasal complex arising from TRN do not seem to fully mature until the end of the second postnatal week (DeBiasi et al., 1997), despite the presence of GABA-containing elements in the thalamus at perinatal ages (Lauder et al., 1986; Bentivoglio et al.,

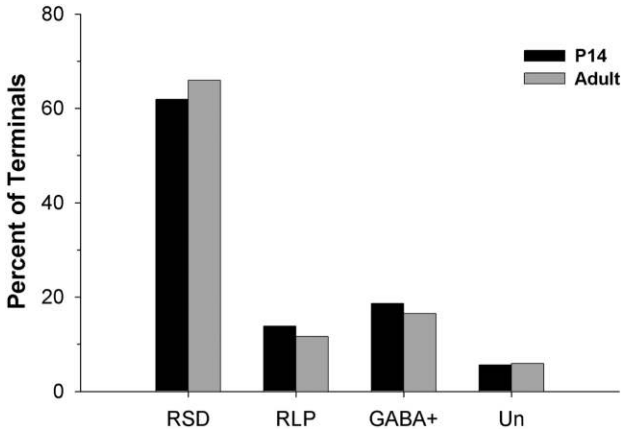

Figure 6. Plot shows the proportion of RSD, RLP, GABAergic, and unclassified terminals at P14 (n = 585) and in adult (n = 558) mouse dLGN. At both ages, the majority of synaptic contacts (61.88–65.95%) were made by RSD profiles; 16.49–18.63% were classified as GABAergic (GABA+) based on immunocytochemical staining, whereas only 11.65–13.85% comprised RLP profiles. The remaining 5.64–5.91% could not be classified (Un).

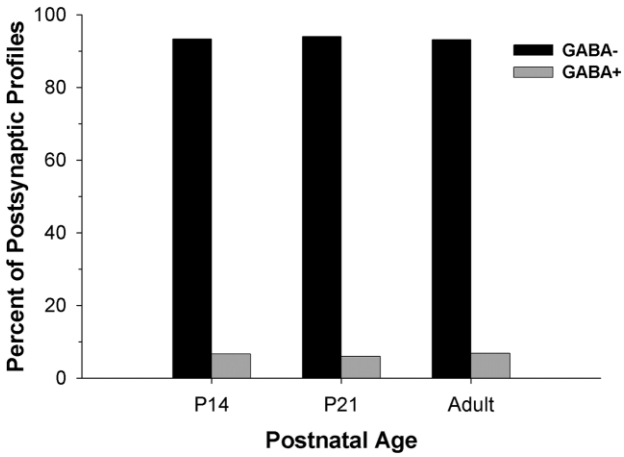

Figure 7. Plot shows the proportion of retinogeniculate terminals at P14, P21, and adult that contact GABAergic (GABA+) and non-GABAergic (GABA-) profiles. At each age, the large majority (>90%) of terminals made contacts with non-GABAergic profiles, but a small percentage also contacted GABAergic F2 profiles. At P14, n = 104, P21, n = 217; and adult, n = 101 RLP profiles.

1991; Laurie et al., 1992.). The latter observation has led to the idea that early GABA expression may serve as a trophic factor rather than an inhibitory neurotransmitter (De Biasi et al., 1997).

Another prevalent feature that emerged at P14 was the presence of RSD profiles. A major source of RSD terminals originates in layer VI of cortex (Esirir et al., 1997a,b). In the mouse, CT axons initially innervate motor and somatosensory nuclei of thalamus before fully innervating the dLGN near the end of the second postnatal week (Jacobs et al., 2007). A similar progression may occur in higher mammals, in which CT axons do not form well-defined RSD profiles until late postnatal ages (Weber and Kalil, 1987; Clasca et al., 1995). The progression of synapse maturation from small undifferentiated (presumably retinal) synaptic terminals to well-defined profiles that reflect both retinal and nonretinal innervation of the dLGN coincides with two major developmental events: the extensive pruning of retinogeniculate connections, and the transition in retinal activity from wave-like patterns of spontaneous firing to visually evoked events. Initially, retinal projections from the two eyes have overlapping terminal fields in dLGN (Jaubert-Miazza et al., 2005). Indeed, at early postnatal ages relay cells are known to receive binocular input and as many as ~2 dozen inputs from separate retinal ganglion cells (Chen and Regehr, 2000; Jaubert-Miazza et al., 2005; Ziburkus and Guido, 2006).

The apparent structural immaturity of retinogeniculate terminals observed at P7 is reflected in their function; synaptic currents elicited by stimulation of retinogeniculate axons at this age are weak and exhibit asynchronous vesicular release (Chen and Regehr, 2000; Hooks and Chen, 2006). Between the first and second postnatal week, retinal projections segregate to form non-overlapping eye-specific domains. The degree of retinal convergence is also greatly reduced so that relay cells receive input from just a few retinal ganglion cells. In fact, based on the percentage of RLP synapses noted at P14, and assuming that most P7 synapses in dLGN are likely to be retinal in origin, there could be as much as a 10-fold reduction in the number of retinogeniculate synapses between P7 and P14. Such large-scale changes in retinogeniculate connectivity have been attributed to spontaneous retinal activity (Torborg and Feller, 2005; Huberman et al., 2008). The nearest-neighbor same eye relations underlying the spatiotemporal patterning of these events is well suited for promoting an activity-based Hebbian form of synaptic plasticity in which temporally correlated activity between pre- and postsynaptic elements leads to synapse strengthening and consolidation, and asynchronous or absence of activity results in synapse weakening and elimination (Torborg and Feller, 2005; Butts et al., 2007).

By the second postnatal week, large-scale retinogeniculate synapse elimination is nearly complete and the remaining synapses undergo significant strengthening (Chen and Regehr, 2000; Hooks and Chen, 2006). By this time the synapses between photoreceptors and bipolar cells have also matured (Takada et al., 2004; Rao et al., 2007), and retinal waves subside and are replaced with visually evoked activity (Demas et al., 2003). Although the functional significance of this developmental sequence remains unclear, perhaps the developmental plan underlying

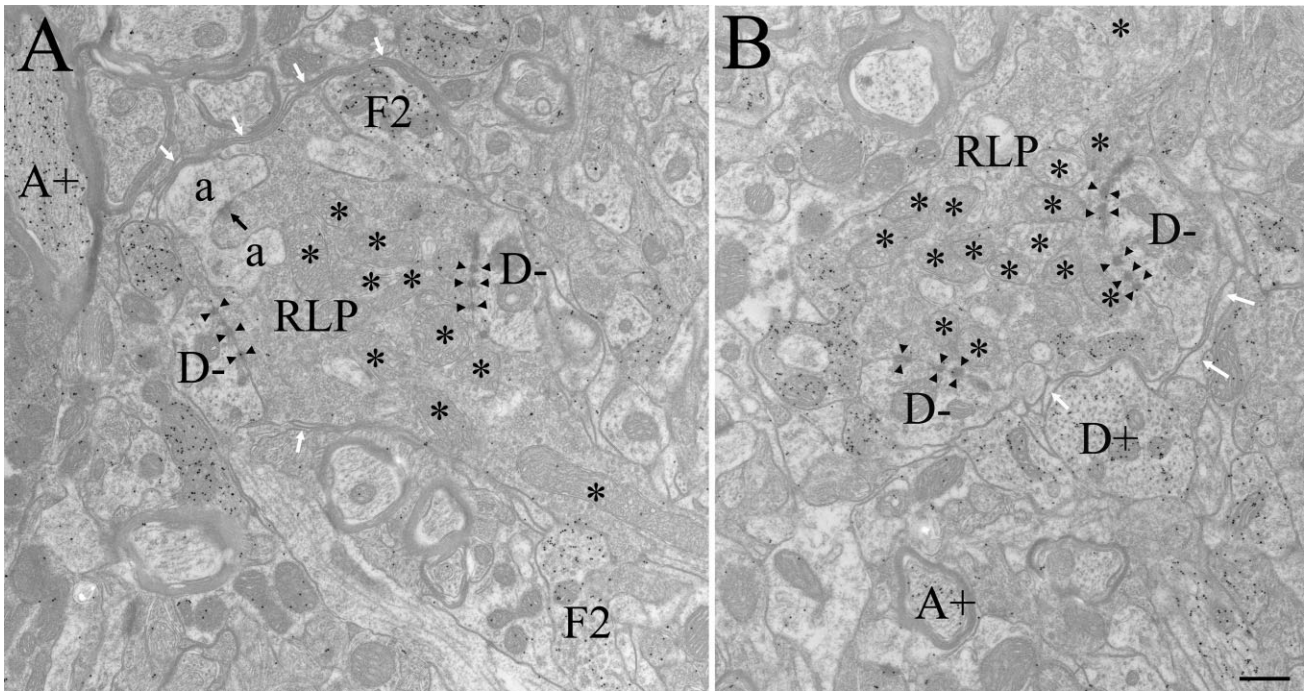

Figure 8. Electron micrographs illustrate retinal terminals in the adult dLGN, identified as RLP profiles: large profiles that contain round vesicles and pale mitochondria (*). In the adult, RLP profiles primarily contacted non-GABAergic dendrites (D-, identified as profiles that contain microtubules and occasional mitochondria, a low density of gold particles, and no synaptic vesicles) via puncta adherentia (arrowheads). Most synaptic contacts (black arrow) were made on dendritic appendages (a, identified as small profiles that contain diffusely organized neurofilaments, no microtubules, few mitochondria, a low density of gold particles, and no synaptic vesicles (as illustrated in **A**), which were often observed to invaginate RLP profiles. RLP profiles also contacted F2 profiles (identified as profiles that contain loosely packed synaptic vesicles and a high density of gold particles (as illustrated in **A**). In the adult, RLP synaptic arrangements were often surrounded by glial lamellae (white arrows). GABAergic dendrites (D+, identified as profiles that contain microtubules and occasional mitochondria, a high density of gold particles, and no synaptic vesicles, as illustrated in **B**) and GABAergic axons (A+, identified as profiles that contain a high density of gold particles and are surrounded by myelin, as illustrated in **A** and **B**) could also be identified. Scale bar = 0.5 μm in B (applies to A,B).

synapse formation in dLGN requires retinal inputs (which drive the response properties of dLGN cells) to be firmly established before inputs that modulate dLGN response properties begin to form synapses in the dLGN. Interestingly, inputs from cortical layer V, which are thought to provide driving inputs in higher order nuclei (Sherman, 2005), are the first to innervate the thalamus, arriving at late embryonic ages and then undergoing a pruning phase at 2–3 weeks postnatal (Clasca et al., 1995).

Finally, it is worth noting that the synaptic architecture of the mouse dLGN is highly conserved. Retinal terminals are in the minority (11–13%), and the overwhelming majority is nonretinal in origin, with 16–19% arising from GABA-containing F-profiles and the remaining 62–66% from RSD terminals. Indeed, these percentages are roughly equivalent to those reported in other species such as the rat, cat, or monkey (Wilson and Hendrickson, 1981; Gabbott et al., 1986; Montero, 1991; Erisir et al., 1998; Van Horn et al., 2000; Li et al., 2003). However, where they do diverge, is in the proportion of RLP contacts on F2 terminals of interneurons, which is far less (10%) than noted in cat (30–40%), monkey (25–30%), and perhaps even the rat (26%). This reduction could be due to the lower density of intrinsic interneurons in the mouse dLGN. Unlike higher mammals (e.g., cat and monkey), in which 20–25% of cells in dLGN are GABAergic (LeVay and Ferster, 1979; Fitzpatrick et al., 1984; Madarasz et al., 1985; Montero and Zempel, 1986; Arcelli et al., 1997; Carden et al., 2000), in rodents only 15–20% of dLGN neurons are reported to be interneurons (Gabbott et al., 1985; Arcelli et al., 1997). Interestingly, this density may even be as low as 10% in mouse (Jaubert-Miazza et al., 2005). Despite this reduced proportion, their presence in the mouse is notable and provides further support for the mouse as a model system of study for synaptic circuitry in dLGN.

ACKNOWLEDGMENTS

The authors thank Mr. Michael A. Eisenback and Ms. Cathie G. Caple for their expert technical assistance with the electron microscopy.

LITERATURE CITED

Arcelli P, Frassoni C, Regondi MC, De Biasi S, Spreafico R. 1997. GABAergic neurons in mammalian thalamus: a marker of thalamic complexity? Brain Res Bull 42:27–37.

Bentivoglio M, Spreafico R, Alvarez-Bolado G, Sanchez MP, Fairen A. 1991. Differential expression of the $GABA_A$ receptor complex in the dorsal thalamus and reticular nucleus: an immunohistochemical study in the adult and developing rat. Eur J Neurosci 3:118–125.

Bickford ME, Wei H, Eisenback MA, Chomsung RD, Slusarczyk AS, Dankowsi AB. 2008. Synaptic organization of thalamocortical axon collaterals in the perigeniculate nucleus and dorsal lateral geniculate nucleus. J Comp Neurol 508:264–285.

Blitz DM, Regehr WG. 2005. Timing and specificity of feedforward inhibition within the LGN. Neuron 45:917–928.

Butts DA, Kanold PO, Shatz CJ. 2007. A burst-based "Hebbian" learning rule at retinogeniculate synapses links retinal waves to activity-dependent refinement. PLoS Biol 5:e61.

Carden WB, Datskovskaia A, Guido W, Godwin DW, Bickford ME. 2000. Development of the cholinergic, nitrergic, and GABAergic innervation of the cat dorsal lateral geniculate nucleus. J Comp Neurol 418:65–80.

Chen C, Regehr WG. 2000. Developmental remodeling of the retinogeniculate synapse. Neuron 28:955–966.

Clasca F, Angelucci A, Sur M. 1995. Layer-specific programs of development in neocortical projection neurons. Proc Natl Acad Sci U S A 92:11145–11149.

Crunelli V, Haby M, Jassik-Gerschenfeld D, Leresche N, Pirchio M. 1988. Cl^-- and K^+-dependent inhibitory postsynaptic potentials evoked by interneurones of the rat lateral geniculate nucleus. J Physiol 399:153–176.

Cucchiaro JB, Bickford ME, Sherman SM. 1991a. A GABAergic projection from the pretectum to the dorsal lateral geniculate nucleus in the cat. Neuroscience 41:213–226.

Cucchiaro JB, Uhlrich DJ, Sherman SM. 1991b. Electron-microscopic analysis of synaptic input from the perigeniculate nucleus to the A-laminae of the lateral geniculate nucleus in cats. J Comp Neurol 310:316–336.

Datskovskaia A, Carden WB, Bickford ME. 2001. Y retinal terminals contact interneurons in the cat dorsal lateral geniculate nucleus. J Comp Neurol 430:85–100.

De Biasi S, Amadeo A, Arcelli P, Frassoni C, Spreafico R. 1997. Postnatal development of GABA-immunoreactive terminals in the reticular and ventrobasal nuclei of the rat thalamus: a light and electron microscopic study. Neuroscience 76:503–515.

Demas J, Eglen SJ, Wong RO. 2003. Developmental loss of synchronous spontaneous activity in the mouse retina is independent of visual experience. J Neurosci 23:2851–2860.

Erisir A, Van Horn SC, Sherman SM. 1998. Distribution of synapses in the lateral geniculate nucleus of the cat: differences between laminae A and A1 and between relay cells and interneurons. J Comp Neurol 390:247–255.

Erisir A, Van Horn SC, Bickford ME, Sherman SM. 1997a. Immunocytochemistry and distribution of parabrachial terminals in the lateral geniculate nucleus of the cat: a comparison with corticogeniculate terminals. J Comp Neurol 377:535–549.

Erisir A, Van Horn SC, Sherman SM. 1997b. Relative numbers of cortical and brainstem inputs to the lateral geniculate nucleus. Proc Natl Acad Sci U S A 94:1517–1520.

Famiglietti EV Jr. 1970. Dendro-dendritic synapses in the lateral geniculate nucleus of the cat. Brain Res 20:181–191.

Famiglietti EV Jr, Peters A. 1972. The synaptic glomerulus and the intrinsic neuron in the dorsal lateral geniculate nucleus of the cat. J Comp Neurol 144:285–334.

Fitzpatrick D, Penny GR, Schmechel DE. 1984. Glutamic acid decarboxylase-immunoreactive neurons and terminals in the lateral geniculate nucleus of the cat. J Neurosci 4:1809–1829.

Gabbott PL, Somogyi J, Stewart MG, Hamori J. 1986. A quantitative investigation of the neuronal composition of the rat dorsal lateral geniculate nucleus using GABA-immunocytochemistry. Neuroscience 19:101–111.

Godement P, Salaun J, Imbert M. 1984. Prenatal and postnatal development of retinogeniculate and retinocollicular projections in the mouse. J Comp Neurol 230:552–575.

Guido W. 2008. Refinement of the retinogeniculate pathway. J Physiol 586:4357–4362.

Guillery RW. 1969. The organization of synaptic interconnections in the laminae of the dorsal lateral geniculate nucleus of the cat. Z Zellforsch Mikrosk Anat 96:1–38.

Guillery RW. 1971. Patterns of synaptic interconnections in the dorsal lateral geniculate nucleus of cat and monkey: a brief review. Vision Res Suppl 3:211–227.

Hamos JE, Van Horn SC, Raczkowski D, Uhlrich DJ, Sherman SM. 1985. Synaptic connectivity of a local circuit neurone in lateral geniculate nucleus of the cat. Nature 317:618–621.

Hamos JE, Van Horn SC, Raczkowski D, Sherman SM. 1987. Synaptic circuits involving an individual retinogeniculate axon in the cat. J Comp Neurol 259:165–192.

Hendrickson AE, Ogren MP, Vaughn JE, Barber RP, Wu JY. 1983. Light and electron microscopic immunocytochemical localization of glutamic acid decarboxylase in monkey geniculate complex: evidence for GABAergic neurons and synapses. J Neurosci 3:1245–1262.

Hooks BM, Chen C. 2006. Distinct roles for spontaneous and visual activity in remodeling of the retinogeniculate synapse. Neuron 52:281–291.

Houser CR, Vaughn JE, Barber RP, Roberts E. 1980. GABA neurons are the major cell type of the nucleus reticularis thalami. Brain Res 200:341–354.

Huberman AD, Feller MB, Chapman B. 2008. Mechanisms underlying development of visual maps and receptive fields. Annu Rev Neurosci 31:479–509.

Jacobs EC, Campagnoni C, Kampf K, Reyes SD, Kalra V, Handley V, Xie YY, Hong-Hu Y, Spreur V, Fisher RS, Campagnoni AT. 2007. Visualization of corticofugal projections during early cortical development in a tau-GFP-transgenic mouse. Eur J Neurosci 25:17–30.

Jaubert-Miazza L, Green E, Lo FS, Bui K, Mills J, Guido W. 2005. Structural and functional composition of the developing retinogeniculate pathway in the mouse. Vis Neurosci 22:661–676.

Lauder JM, Han VK, Henderson P, Verdoorn T, Towle AC. 1986. Prenatal ontogeny of the GABAergic system in the rat brain: an immunocytochemical study. Neuroscience 19:465–493.

Laurie DJ, Wisden W, Seeburg PH. 1992. The distribution of thirteen $GABA_A$ receptor subunit mRNAs in the rat brain. III. Embryonic and postnatal development. J Neurosci 12:4151–4172.

LeVay S, Ferster D. 1979. Proportion of interneurons in the cat's lateral geniculate nucleus. Brain Res 164:304–308.

Li J, Wang S, Bickford ME. 2003. Comparison of the ultrastructure of cortical and retinal terminals in the rat dorsal lateral geniculate and lateral posterior nuclei. J Comp Neurol 460:394–409.

Lieberman AR, Webster KE. 1974. Aspects of the synaptic organization of intrinsic neurons in the dorsal lateral geniculate nucleus. An ultrastructural study of the normal and of the experimentally deafferented nucleus in the rat. J Neurocytol 3:677–710.

Madarasz M, Somogyi G, Somogyi J, Hamori J. 1985. Numerical estimation of gamma-aminobutyric acid (GABA)-containing neurons in three thalamic nuclei of the cat: direct GABA immunocytochemistry. Neurosci Lett 61:73–78.

Montero VM. 1991. A quantitative study of synaptic contacts on interneurons and relay cells of the cat lateral geniculate nucleus. Exp Brain Res 86:257–270.

Montero VM, Scott GL. 1981. Synaptic terminals in the dorsal lateral geniculate nucleus from neurons of the thalamic reticular nucleus: a light and electron microscope autoradiographic study. Neuroscience 6:2561–2577.

Montero VM, Singer W. 1985. Ultrastructural identification of somata and neural processes immunoreactive to antibodies against glutamic acid decarboxylase (GAD) in the dorsal lateral geniculate nucleus of the cat. Exp Brain Res 59:151–165.

Montero VM, Zempel J. 1986. The proportion and size of GABA-immunoreactive neurons in the magnocellular and parvocellular layers of the lateral geniculate nucleus of the rhesus monkey. Exp Brain Res 62:215–223.

Mooney R, Penn AA, Gallego R, Shatz CJ. 1996. Thalamic relay of spontaneous retinal activity prior to vision. Neuron 17:863–874.

Oertel WH, Graybiel AM, Mugnaini E, Elde RP, Schmechel DE, Kopin IJ. 1983. Coexistence of glutamic acid decarboxylase- and somatostatin-like immunoreactivity in neurons of the feline nucleus reticularis thalami. J Neurosci 3:1322–1332.

Ohara PT, Sefton AJ, Lieberman AR. 1980. Mode of termination of afferents from the thalamic reticular nucleus in the dorsal lateral geniculate nucleus of the rat. Brain Res 197:503–506.

Patel NC, Bickford ME. 1997. Synaptic targets of cholinergic terminals in the pulvinar nucleus of the cat. J Comp Neurol 387:266–278.

Rafols JA, Valverde F. 1973. The structure of the dorsal lateral geniculate nucleus in the mouse. A Golgi and electron microscopic study. J Comp Neurol 150:303–332.

Rao A, Dallman R, Henderson S, Chen CK. 2007. Gbeta5 is required for normal light responses and morphology of retinal ON-bipolar cells. J Neurosci 27:14199–14204.

Rapisardi SC, Miles TP. 1984. Synaptology of retinal terminals in the dorsal lateral geniculate nucleus of the cat. J Comp Neurol 223:515–534.

Rinvik E, Ottersen OP, Storm-Mathisen J. 1987. Gamma-aminobutyrate-like immunoreactivity in the thalamus of the cat. Neuroscience 21:781–805.

Robson JA, Mason CA. 1979. The synaptic organization of terminals traced from individual labeled retino-geniculate axons in the cat. Neuroscience 4:99–111.

Sherman SM. 2004. Interneurons and triadic circuitry of the thalamus. Trends Neurosci 27:670–675.

Sherman SM. 2005. Thalamic relays and cortical functioning. Prog Brain Res 149:107–126.

Sherman SM, Guillery RW. 2002. The role of the thalamus in the flow of information to the cortex. Philos Trans R Soc Lond B Biol Sci 357:1695–1708.

Szentagothai J, Hamori J, Tombol T. 1966. Degeneration and electron microscope analysis of the synaptic glomeruli in the lateral geniculate body. Exp Brain Res 2:283–301.

Takada Y, Fariss RN, Tanikawa A, Zeng Y, Carper D, Bush R, Sieving PA. 2004. A retinal neuronal developmental wave of retinoschisin expression begins in ganglion cells during layer formation. Invest Ophthalmol Vis Sci 45:3302–3312.

Torborg CL, Feller MB. 2005. Spontaneous patterned retinal activity and the refinement of retinal projections. Prog Neurobiol 76:213–235.

Van Horn SC, Erisir A, Sherman SM. 2000. Relative distribution of synapses in the A-laminae of the lateral geniculate nucleus of the cat. J Comp Neurol 416:509–520.

Wang S, Bickford ME, Van Horn SC, Erisir A, Godwin DW, Sherman SM. 2001. Synaptic targets of thalamic reticular nucleus terminals in the visual thalamus of the cat. J Comp Neurol 440:321–341.

Wang S, Eisenback M, Datskovskaia A, Boyce M, Bickford ME. 2002. GABAergic pretectal terminals contact GABAergic interneurons in the cat dorsal lateral geniculate nucleus. Neurosci Lett 323:141–145.

Weber AJ, Kalil RE. 1987. Development of corticogeniculate synapses in the cat. J Comp Neurol 264:171–192.

Wilson JR, Hendrickson AE. 1981. Neuronal and synaptic structure of the dorsal lateral geniculate nucleus in normal and monocularly deprived *Macaca* monkeys. J Comp Neurol 197:517–539.

Wilson JR, Friedlander MJ, Sherman SM. 1984. Fine structural morphology of identified X- and Y-cells in the cat's lateral geniculate nucleus. Proc R Soc Lond B Biol Sci 221:411–436.

Ziburkus J, Guido W. 2006. Loss of binocular responses and reduced retinal convergence during the period of retinogeniculate axon segregation. J Neurophysiol 96:2775–2784.

Ziburkus J, Lo FS, Guido W. 2003. Nature of inhibitory postsynaptic activity in developing relay cells of the lateral geniculate nucleus. J Neurophysiol 90:1063–1070.